Journal of Power Sources 196 (2011) 6695–6702

Contents lists available at ScienceDirect

Journal of Power Sources

journal homepage: www.elsevier.com/locate/jpowsour

Role of the binder on the failure mechanism of Si nano-composite electrodes for Li-ion batteries

D. Munao*, J.W.M. van Erven, M. Valvo, E. Garcia-Tamayo, E.M. Kelder

NanoStructured Materials, Department of Chemical Engineering, TUDelft, 2628BL Delft, The Netherlands

ARTICLE INFO

Article history:
Received 14 September 2010
Received in revised form
12 November 2010
Accepted 12 November 2010
Available online 19 November 2010

Keywords:
Si
Nano-composite
Thin-film
Fading mechanism

ABSTRACT

In this work a novel method is used to fabricate uniform thin layer electrodes based on nano-silicon composite material. The manufacture process, based on a combination of Laser assisted Chemical Vapor Pyrolysis and Electro-Spray Deposition, allows the forming of highly uniform and highly porous surface electrodes. By controlling the particle synthesis and deposition parameters it is possible to obtain samples that are highly reproducible in terms of their morphology. Electrosprayed nano-composite electrodes show high specific capacity. The capacity retention of these types of electrodes is strongly dependant on the binder's nature. The capacity fading mechanism has been further investigated and we suggest a simple mechanical model, which is supported by one of the two CMC binding mechanism already proposed in literature.

1. Introduction

Silicon is widely considered as one the most promising anode materials for Li-ion batteries due to its alloying reaction with Li. The packing density of the Li atoms within the $Li_{22}Si_5$ alloy is even higher than the one exhibited by the structure of metallic Li [1]. The high density of the Li atoms in the Si structure brings about the highest theoretical capacity (4200 mAh g^{-1}) [2]. Despite that, Si-based electrodes suffer from poor cyclability due to severe mechanical stresses involved in the alloying and de-alloying processes. These are responsible for macro-fractures of the host electrode structure and loss of electrical contact [3]. Recently, considerable effort from both academic and industrial research has been invested into this problem in order to overcome these drawbacks. The ultimate goal would be to find suitable applications for Li-ion batteries in sustainable mobility and electric vehicle traction. Several approaches have been taken to deal with the poor cyclability issue, namely: forming composite materials in which active alloy or metal particles are finely dispersed in an inactive or active solid matrix which buffers the expansion of the active phase [4–8]; using nano-particles that can sustain the physical strains upon Li uptake/removal [9–12]; using thin film technology to fabricate novel electrodes [13–16]; using selected binders that maintain the integrity of the electrode by maintaining the contact between the active material (alloy/metal), the conducting additive (carbon), and the current collector making use of suitable surface interactions [17–21].

In this work Si nano-particles are produced by means of a newly designed Laser assisted Chemical Vapor Pyrolysis (LaCVP) reactor. LaCVP is a versatile process in which nano-particles are formed from the thermal decomposition of one or more gaseous reactants [22,23]. The decomposition is initiated and assisted by the energy of a CO_2 laser beam. Gases are fed into the reactor by means of two concentric rectangular nozzles. The new design of the reactor used allows the production of pilot scale quantities of evenly distributed spherical Si nano-particles. These particles were used to fabricate composite electrodes, of which the structural and morphological properties were investigated before and after cycling. The electrode fabrication process is carried out with the extremely versatile Electro-Spray Deposition (ESD) technique. Several studies have been carried out and promising results have shown the potential of this technique for developing both positive and negative electrodes, as well as solid electrolytes [24–26]. The possibility of direct synthesis or deposition of nano-structured electrode materials onto current collectors is particularly attractive, especially for thin film preparation. ESD allows uniform coating of thin layers at low temperatures and can be easily scaled up into an industrial single-step battery assembly process.

Here, the electrochemical performance of such nano-structured Si electrodes is investigated and further considerations on the origin of the capacity fading mechanism are proposed.

* Corresponding author. Tel.: +31 6 48315699; fax: +31 15 2575979.
E-mail address: d.munao@tudelft.nl (D. Munao).

0378-7753/$ – see front matter © 2010 Elsevier B.V. All rights reserved.
doi:10.1016/j.jpowsour.2010.11.072

Table 1
Electrospray parameters.

Sample name	Si–PVdF	Si–CMC	Si–CMC–C
Polymer	Polyvinylidene difluoride (Solef 1015)	Carboxymethylcellulose (Alpha Aesar)	Carboxymethylcellulose (Alpha Aesar)
Si to polymer weight ratio	7:3	3:1, 1:1	1:1:1
Solvent	N-methyl-2-pyrrolidone (MERK)	H_2O (milli-q): 2-propanol (J.T. Baker) 1:1	H_2O (milli-q): 2-propanol (J.T. Baker) 1:1
Voltage [kV]	8.3	10.5	11
Substrate temperature [°C]	280	100	100
Flow rate [ml h^{-1}]	0.1	0.1	0.3
Sprayed volume [ml]	0.03	0.06	0.04

2. Materials and methods

Silicon nano-particles were synthesized by LaCVP. Particles synthesis details and the complete geometry of the reactor are given elsewhere [27]. SiH_4, diluted with N_2, was used as reactant for the production of Si nano-particles for the inner nozzle and N_2 was used as sheath gas for the outer nozzle. Synthesis parameters, such as gas flow rates, pressure and laser power, used during the particles production were respectively: 0.24 l min^{-1} of SiH_4 from the inner nozzle, 2.16 l min^{-1} of N_2 from the inner nozzle, 11.34 l min^{-1} of N_2 from the outer nozzle, 800 mbar and 510 W. Electrodes were prepared by electro-spraying a precursor ink onto a heated substrate. Precursor inks were prepared by ultrasonicating the silicon nano-particles in a polymer solution. The composition for each prepared sample is specified in Table 1. Si powders were pre-treated in the case of samples Si–CMC and Si–CMC–C (see Table 1) in order to promote the chemical activation of the surface. 500 mg of Si nano-particles were dispersed in 50 ml of Acetic Acid (Baker Analyzed, 99–100%), sonicated for 10 min, centrifuged for 3 h at 3000 rpm (Automatic Servall Superspeed), collected and dried under air at room temperature. After the surface activation procedure, an increase in mass of ~200% was observed on the Si powder. The mass increase is attributed to the physical absorption of the acetic acid on the particle surface. The surface activation process was chosen as an alternative chemical route in order to increase the affinity between the CMC and the Si nano-particles. It is well known [28], that CMC solubility it is strongly reduced in an acidic water media. In this way, the pH is reduced locally, at the particles surface, and no phase segregation was observed during the preparation of the ink.

Precursor inks were loaded into a glass syringe (Fortuna Optima), which was connected through a chemically resistant hose (Watson-Marlow) to a stainless steel nozzle (EFD Ultra). The nozzle, on its turn, was connected to the positive pole of a high voltage power supply (HCN 14-12500). A syringe pump (Kd Scientific) enabled the feeding of the precursors to the nozzle at a controlled flow rate. The distance between the nozzle and the substrate was kept the same in all the experiments (i.e. 20 mm), and measured via a built-in digital calliper. The temperature of the substrate where the sample was mounted was maintained by a thermostat. The temperature was constantly monitored via thermocouples, in order to control the heating process by adjusting the power supplied to the hot plate. The temperature was set above the boiling temperature of the solvent used to prepare the precursor ink. The electro-spray process took place under air and all the significant parameters for the electrode preparation are listed in Table 1 for each sample prepared. The precursors were sprayed directly onto the lower part of a coin cell. For this purpose, empty stainless steel cans (i.e. CR2320 – Hosen) were carefully weighed on a digital balance (Sartorious) with an accuracy of 10^{-5} g before being placed onto the heated substrate holder. Selective coating on a circular area concentric to the rim of the can was achieved by applying a cardboard mask with a punched hole of 14 mm diameter. After the coating process, the coin cells cans were weighed again on the balance and the amount of deposited composite material was determined via the mass difference. The typical weight of the composite layer was between 0.8 and 1.2 mg. The samples were dried for one night at 70 °C under vacuum. It is worth mentioning that the resulting electrodes do not need any further treatment and that they can be directly sealed in a full battery assembly by simply adding the remaining parts (i.e. electrolyte-soaked separator, lithium disk, spring, gasket and stainless steel lid).

Coin cells were assembled inside a He filled glove box (Mbraun) using metallic Li as negative electrode, $LiPF_6$ in EC:DMC 1:1 mixture (Mitsubishi Chemical) as electrolyte and the Si nano-composite as the positive electrode. The cells were cycled in a Maccor (S4000) battery tester in order to assess the electrode behavior in terms of capacity and cycling performance. All the samples were cycled at the same constant current rate (0.1 mAh mg^{-1} of active material) in a voltage window between 0.06 and 1 V at room temperature. Scanning Electron Microscopy (SEM) was carried out on a Philips XL20 microscope. The electrode morphology was studied before and after cycling in order to evaluate the overall mechanical resistance of the layers upon the volume expansion induced by the galvanostatic tests.

Transmission Electron Microscopy (TEM, coupled with Energy Dispersive Spectroscopy, EDS) was carried out to study the morphology, size and crystallinity of the as-produced nano-particles. TEM was performed using a FEI Tecnai TF20 electron microscope with a field emission gun as the source of electrons operated at 200 kV. TEM samples were prepared by placing a few droplets of a suspension of ethanol and ground silicon on a carbon polymer (Quantifoil) supported by a copper grid, followed by drying at ambient condition in order to evaporate the ethanol. EDS elemental analysis was performed using an Oxford Instruments EDX system. The phase analysis of synthesized powders was performed by using a BRUKER-AXS D8-Advance X-ray Diffractometer that was operated at 40 kV and 40 mA equipped with a Cu Kα radiation source. The scan range was chosen as $25^\circ < 2\theta < 60^\circ$ with a scan speed of 10 s $step^{-1}$ and 0.05 step size. The surface properties were investigated via Fourier Transform Infra-Red spectroscopy (FTIR, Perkin Elmer Spectrum one). Samples were prepared by mixing the composite electrode material with dry KBr and forming a solid pellet that was analyzed in transmission mode under air. Thermal Gravimetric Analysis (TGA, PerkinElmer TGA7) was carried out to study the oxidation rate of the Si nano-particles in air. TGA was performed in air at a heating rate of 10 °C min^{-1}.

3. Results and discussion

3.1. Si nano-particles characterization

The diffraction pattern of Fig. 1 indicates that the Si nano-particles generated by LaCVP are crystalline. Three broad peaks observed around 28°, 47° and 56° match respectively with the characteristic planes (1 1 1), (2 2 0) and (3 1 1) of the Si lattice, according to the crystallographic data (i.e. JCPDS No. 75-0590). No traces of crystalline oxides are detected in the spectrum, suggesting that the surface oxidation of the particles most likely resulted in an amor-

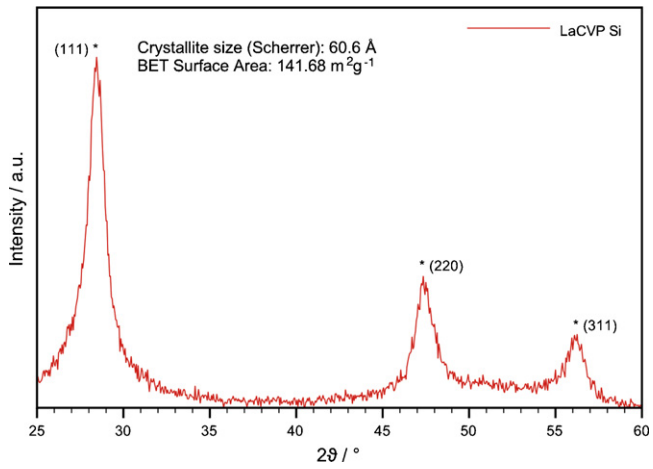

Fig. 1. XRD diffraction pattern of the as-produced Si nano-particles.

phous SiO_x layer only, which accounts for the stability of the Si nano-particles in air. Such a native oxide amorphous layer is also found from both the TEM images and the FTIR surface analysis.

The chemical stability of the Si nano-particles towards oxidation is confirmed by the thermal analysis. TGA (Fig. 2) reveals that no mass is gained up to 200 °C. In addition to that, no change in color was observed on a time-scale of 6 months after synthesis, storing the powder under ambient atmospheric conditions.

The morphology and structure of the nano-particles is shown in the TEM image, Fig. 3. A typical size of 10 nm is observed for most of the particles, which also exhibit a rather homogeneous size distribution. The particles are more or less spherical and their mean size is in good agreement with both the surface area given from BET analysis and the crystallite size calculated from the XRD spectrum via the Scherrer formula (9.1 and 6 nm respectively, Fig. 1). Of course the latter method does not take the outer amorphous layer thickness into consideration. The thickness of the amorphous layer is estimated to be between 1 and 2 nm from TEM analysis.

3.2. Composite electrode characterization

A typical cross-section of the ES deposited electrode is shown in Fig. 4. The thickness of the electrode typically ranges from 10 to 20 μm. The electrode thickness is homogenous throughout the entire sprayed surface. The thickness can be simply controlled by adjusting the deposition time on the substrate. For the compositions studied in this work the adhesion on the stainless steel

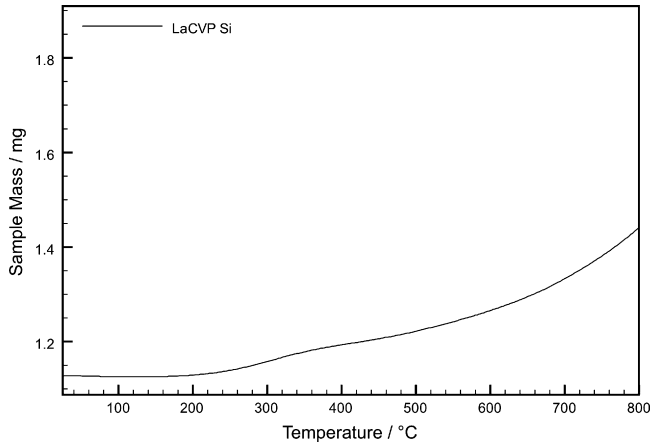

Fig. 2. TGA of the as-produced Si nano-particles.

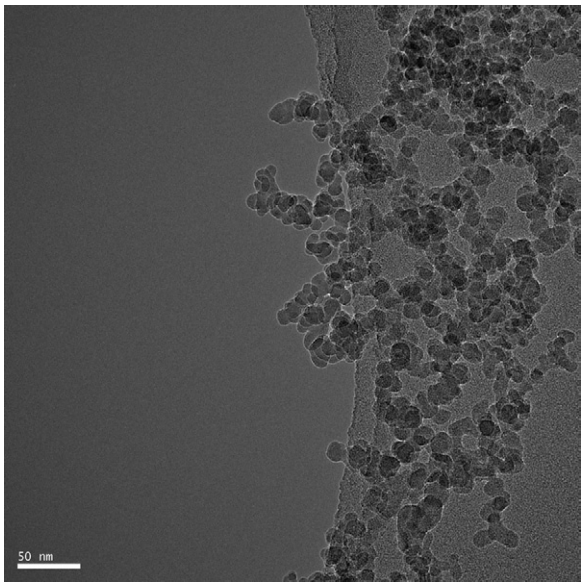

Fig. 3. TEM image of the as-produced Si nano-particles.

support is shown to be very good, for both the PVdF and the CMC based composite electrodes. Visual observation of the thin layer shows a homogeneous, uniformly colored and adherent layer. The deposited layers are shown to be highly porous, and the porosity is observed on the surface as well as in the bulk of the electrode (Fig. 4, magnification on the right corner). Porosity is a highly desired feature for this types of electrodes, as it maximizes the contact between the active material surface and the electrolyte and guarantees free space for the volume expansion upon cycling [29]. Porosity is achieved with the combination of the novel ES fabrication process and the use of nano-sized Si particles. During the ES process, the shear stress on the liquid surface, due to the electric field, causes the formation of a jet and its subsequent disintegration into highly charged tiny droplets, which in some cases can go down to the nanometer scale in size. The electric field accelerates these droplets towards the substrate and the evaporation of the solvent takes place at high rates due to the small droplet size [30]. The result is a highly porous nano-structured electrode.

The first 35 cycles of the galvanostatic test are shown in Fig. 5 for sample Si–PVdF, Si–CMC (1:1) and Si–CMC–C (Fig. 5A, B and C respectively). As is clear from all the results shown here, these novel electrodes show superior performance, in terms of both capacity and capacity retention, when compared to micron-size Si particles

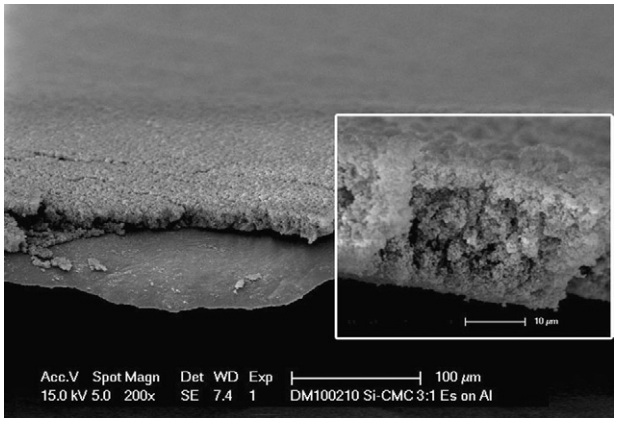

Fig. 4. SEM image of ES Si–CMC 3:1 sample deposited on Al substrate. Right corner shows a magnified section of the thin layer.

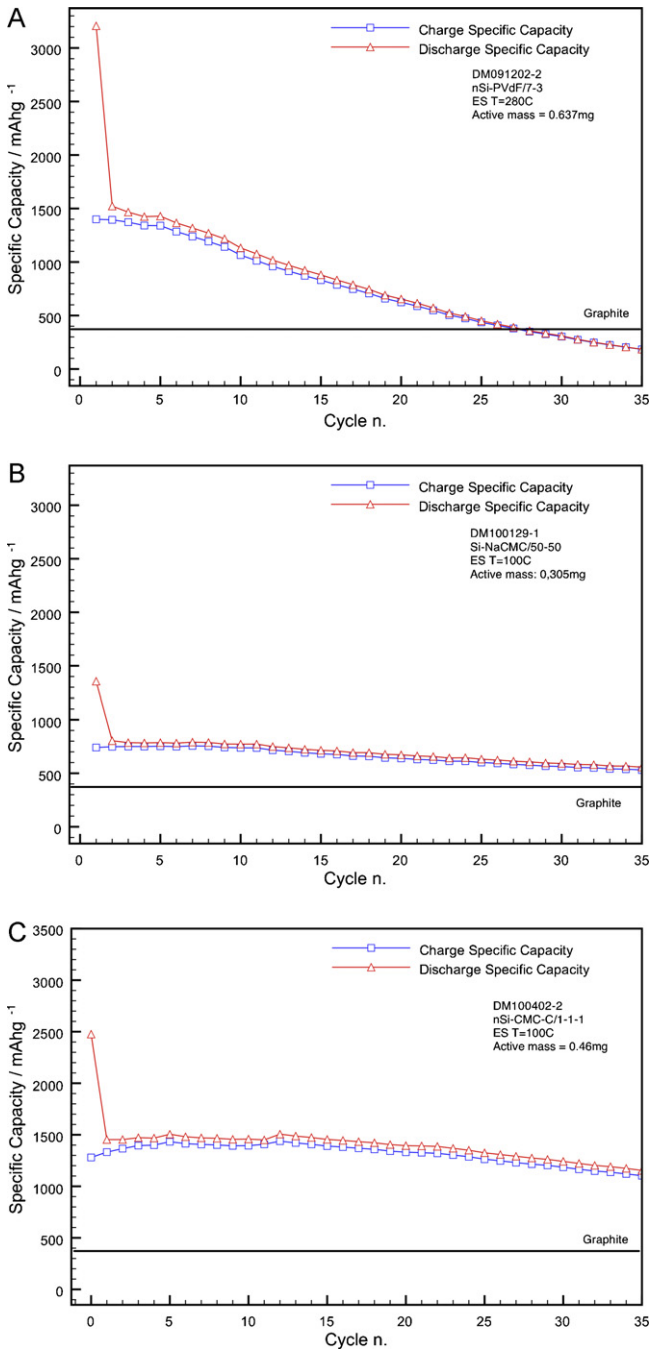

Fig. 5. Galvanostatic tests performed on composite electrodes. (A) Si–PVdF sample. (B) Si–CMC (1:1) sample. (C) Si–CMC–C sample.

based electrodes [31]. Previous studies in our laboratories showed that electrodes based on micron-size particles have a capacity retention of only 4.8% at the 25th cycle. It is important to keep in mind that all the specific capacities discussed here refer to the mass of the active material (i.e. Si), i.e. the entire mass of the composite material is not taken into consideration. However, for practical reason (i.e. application in a real Li-ion battery) it is important to remind that the overall composite weight influences the real gravimetric capacity of the electrode. Therefore, a technological issue of great importance is to find a compromise between having a high capacity and a long device lifetime with a low additives load. Since this is not the aim of the work, the attention is here focussed on the fundamental aspects of the active material capacity and capacity retention only.

The first sample (Fig. 5A) almost reaches the theoretical Si capacity in the first discharge. After the first irreversible capacity drop, estimated to be around 50% of the initial capacity, which is attributed to the Solid Electrolyte Interface (SEI) formation and to the LiO_2 formation [32], the capacity is maintained at a relatively high value (i.e. 1300 mAh g^{-1}, corresponding to 910 mAh g^{-1} of composite material) for the first 10 cycles.

This behavior has already been observed in literature and it is attributed to the thermal activation of the PVdF [33]. PVdF apparently forms a better distribution on the surfaces of the Si particles after heat-treatment, as supported by optical observations and adhesion tests. For this reason, in the case of the Si–PVdF sample a heating temperature of 280 °C has been adopted, despite the boiling temperature of the NMP being 202 °C. After the 10th cycle the capacity starts to fade progressively, going below the one for graphite, which is considered here as the commercial standard, after the 27th cycle.

The second sample (Fig. 5B) shows already a much better cyclability compared to the Si–PVdF sample. After the first irreversible capacity drop, estimated to be around 50% of the initial capacity value, the cycle versus cycle number profile remains almost flat. After the 12th cycle a small capacity fading starts to be visible. Although the initial capacity is not high compared to the theoretical value, the capacity after the 35th cycle is still higher than the one for graphite. The small initial specific capacity value (i.e. 1400 mAh g^{-1}, corresponding to 700 mAh g^{-1} of composite) is attributed to kinetic limitations caused by the high electrical resistance of the composite material.

This issue is clearly solved as soon as the electronic conductivity of the composite is enhanced by the presence of the carbon additive. The third sample (Fig. 5C) shows, in fact, the same cyclability performances offered by the Si–CMC sample but with capacity values that are almost doubled. It is worth noting that, in the case of the Si–CMC–C sample the capacity is maintained at the remarkable value of 1153 mAh g^{-1} up to the 35th cycle (corresponding to 380 mAh g^{-1} of composite). It is important to remark that, although the galvanostatic procedure adopted is the same for all the three samples studied here, the voltage limitation does not imply necessarily the same level of lithium insertion. Due to kinetic factors (i.e. different over potentials) different samples show different capacities at the same cutoff voltage. Practically, also the volumetric response of the matrix will be different. For a more accurate comparison, which takes into account the same volume change in the structure, the galvanostatic test should be capacity limited rather than voltage limited.

These galvanostatic tests show very promising results for the use of nano-Si based composite structures for negative Li-ion batteries electrodes. At the same time the fundamental role of the binder, and

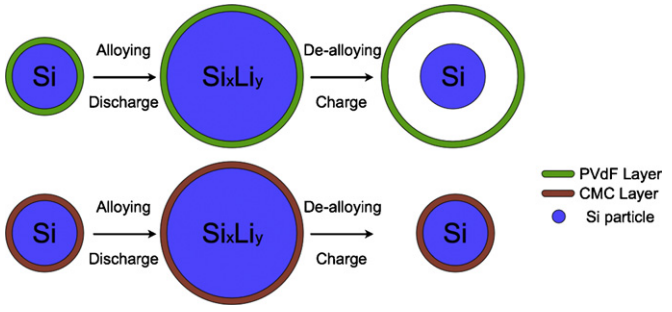

Fig. 6. Proposed capacity fading mechanism for Si composite electrodes. Depending on the chemical affinity between the polymer and the particle surface the overall mechanical stability of the composite, or in other words, the inner electrical wiring will be maintained upon tensile stress induced by the alloying process. In this case CMC is shown to be much more adherent to the particles surface compared to PVdF despite its lower mechanical elasticity.

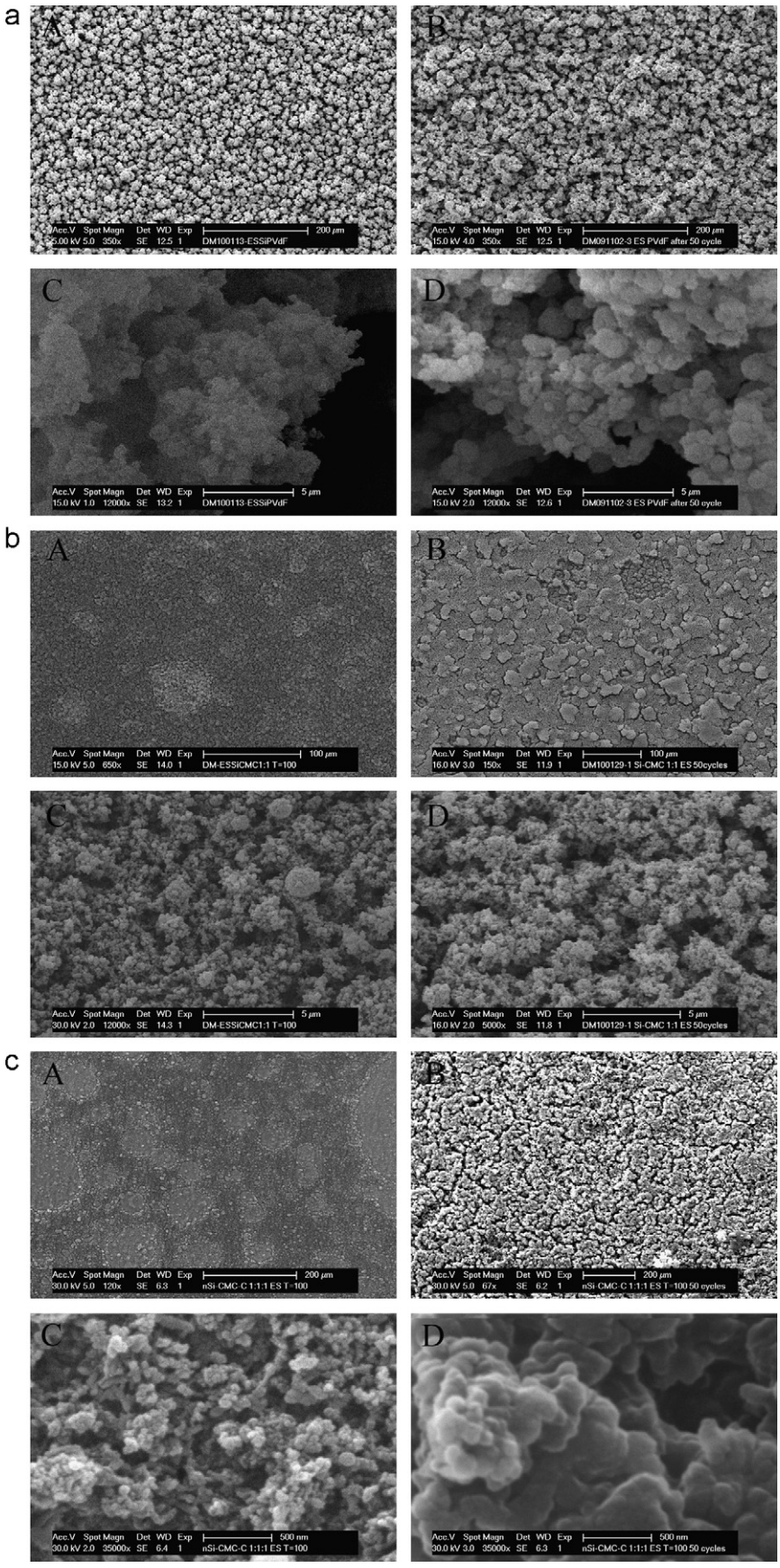

Fig. 7. (a–c) SEM image of Si–PVdF, Si–CMC (1:1) and Si–CMC–C respectively. Figures A and B show an overview of the samples before and after cycling respectively. Figures C and D show a close up of the composites before and after cycling respectively.

in particular of the interaction between the binder and the active material particles is confirmed. Among the multitude of polymeric materials that can act as binders, one would naively believe that the most efficient ones will be those presenting the highest elasticity and resistance to mechanical stretching. Surprisingly, PVdF, while having high deformation capacities, specified to be from 20 to 50% from the supplier (elongation at break, 50 mm min^{-1}, ASTM D638, Solef 1015 PVdF), does not improve the cyclability to the expected extent. This observation obviously suggests that elasticity is not the key issue, but rather the nature of the bonding with the active particles. This was recently pointed out by Li et al. who show that carboxyl-methyl-cellulose (CMC), despite having a high stiffness and a small elongation at break (5–8%), appears to be the best binder to date for the stability of the Li–Si reaction [34]. Here we propose a simple mechanical model that explains the fading mechanism, based on the interaction between the polymer and the particle surface (see Fig. 6). During the first step of the electrochemical alloying the Si particles are growing in size and the binder, which is coating the particles surface, is following the morphological change induced by the volume expansion. During the second step, the lithium is extracted from the alloy and the particles shrink down to the initial size. Here two different cases are made, the first one in which the polymer is not able to follow the volume change and the second one, in which, due to the specific interaction between the particle surface and the binder, the polymer follows the morphological change induced by the cycling procedure. It is important to point out that the scheme shown in Fig. 6 only represents the contact at the interface between the polymer and the particle. No assumptions are made on the volume of polymer involved in the process. The real physical situation is better described by particles embedded in a 3D network polymeric matrix.

The model proposed here (Fig. 6) is supported by SEM observation of the electrode morphology. The electrode morphology was studied before and after 50 cycles. The results are shown in Fig. 7. The Si–PVdF sample (Fig. 7a) shows a well-defined micro-structure with a high porous texture. Its structural unit can be identified in a cauliflower-like configuration, which is nano-structured at the sub-micron level. The Si–CMC (1:1) sample morphology (Fig. 7b) looks much more homogenous compared to the Si–PVdF sample, with pores and voids that are smaller and more equally distributed throughout the entire electrode surface. In order to confirm the mechanical model proposed here it is of great interest to look at the electrode morphology after cycling, paying special attention to both the macro-structure and the micro-structure modification that are exhibited by the thin layers after repeated charge-discharge cycles. The Si–PVdF sample macro-structure looks almost unaltered compared to the as-prepared electrode (Fig. 7a). The cauliflower-like structure is still visible after 50 cycles confirming of the good tensile properties of the fluorinated binder. On the other hand, despite the good cycling ability of the cellulose composite, the Si–CMC (1:1) texture (Fig. 7b) looks severely damaged after the galvanostatic test. The electrode surface looks cracked and heterogeneous compared to the as-prepared electrode.

The CMC binder evidently cannot sustain the large volume expansion that the particle aggregates are undergoing upon cycling.

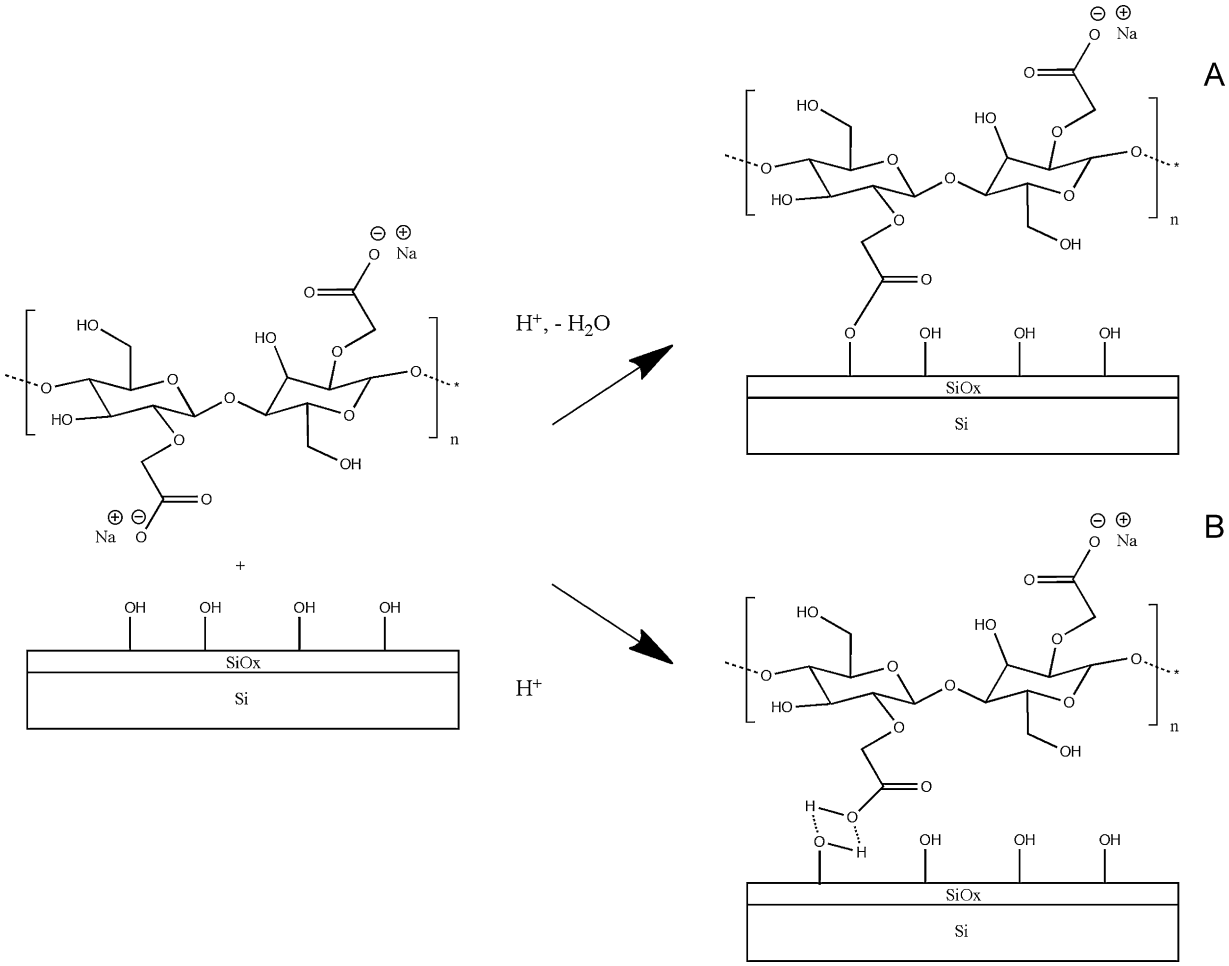

Fig. 8. Proposed CMC bonding mechanism with the Si nano-particles surface. Figure A shows the ester-like covalent bond formation while figure B depicts the H-bond formation.

However as the capacity is maintained, we can conclude that the electrical contact is not lost and remains to be effective at the micro-scale.

A close up view of the electrodes microstructure reveals similar features. The polymer-particle aggregates are larger in the Si–PVdF (Fig. 7a) sample compared to the Si–CMC sample (Fig. 7b). Even though PVdF has better elastic properties compared to CMC apparently it is not able to follow the particle volume change and detaches from them at the surface (as shown in Fig. 6).

On the CMC binding mechanism several hypotheses has been formulated so far. It is important to try to figure out the specificity of the interaction between the Si particles and the CMC and why this interaction allows the conservation of the electrical contact despite the large volume change. The CMC polymer chains are decorated with many polar groups and it is well known that carbohydrate-based polymers undergo many inter- and intra-chain hydrogen-bond interactions [35,36] also depending on the presence of water and on mechanical stress [37]. Some authors have suggested the formation of a strong ester-like covalent bond resulting from the reaction of the carboxyl groups with the hydroxyl group at the surface of the thin SiO_x shell surrounding the Si particles [38] as depicted in Fig. 8A.

Other authors proposed, on the basis of NMR studies, a weak bond formation between the polymeric chain and the Si nano-particles via hydrogen bond interactions (Fig. 8B) [39]. This hypothesis seems to be the most favorable one, as the weakness of the bond would allow the self-healing process of the electrode upon volume change. Hydrogen bonds, in fact, can break and reform dynamically in the presence of residual water [40]. This would further explain the SEM results shown in Fig. 7, where the polymer, in accordance with the dimensions of the observed features, is closely bound to the Si nano-particles. Further evidence that the ester-like covalent bond is not formed during the synthesis process is found from FTIR measurements. FTIR spectra of the used powders are shown in Fig. 9. Two samples were analyzed: CMC powder as a reference and the pre-treated Si nano-powders/CMC mixture. The second sample was prepared by drying the respective precursor inks under air at 100 °C. As is clear from the spectra the peaks attributed to the carboxyl function (1624 and 1410 cm^{-1}) are slightly shifted to lower wave numbers but are still present and clearly visible.

This, together with the formation of a little shoulder in the carbonyl region (1200 cm^{-1}), would suggest the presence of a new, weak interaction in proximity of that chemical function [41]. On the other hand, the IR region involved in an ester bond formation (1735–1750 cm^{-1}) stays unaltered, excluding the possibility of a covalent ester bond between the CMC and the Si surface.

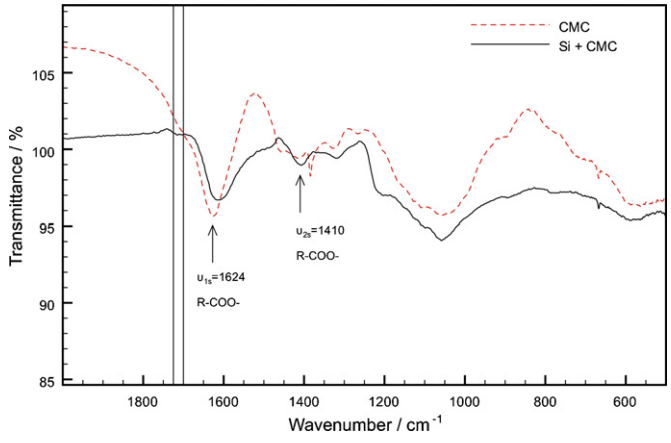

Fig. 9. FTIR spectra of the dry powders used during the electrode preparation.

4. Conclusions

In this work we present novel methods to assemble thin layer composite electrodes based on Si nano-particles. Strategies that are adopted here to over come the capacity fading issue are reducing the particle size down to 10 nm and creating composite thin films using selected binders. Adjusting the physical parameters of the ES fabrication technique allows control of the morphology, thickness and texture of the deposited layers. Three main composites have been studied, based on Si–PVdF, Si–CMC and Si–CMC–C respectively. The fabricated electrodes show good homogeneity, perfect adhesion on the substrate and high porosity. Promising electrochemical results were found, in particular the Si–CMC–C sample has shows capacity retention close to 99% up to the 35th cycle. The capacity fading mechanism has been further investigated and we suggest a simple mechanical model, which is supported by one of the two CMC binding mechanism already proposed in literature. Hydrogen-bond formation between the CMC and the surface of the nano-particles and the dynamic nature of this weak interaction are responsible for the self-healing process that occurs at the sub-micron scale, where the electrical contact does not appear to be lost. As no specific interaction between PVdF and the surface of the Si nano-particle is expected, the capacity of such nano-composite electrodes tends to fade much more rapidly.

Acknowledgments

The authors acknowledge the DEMO section, TUDelft, for the valuable and constant support given during the set up of the LaCVP instrument. The authors would also like to thank the National Center of HRTEM and in particular Patricia Kooyman for her precious support on TEM measurements. Special thanks are given to Prof. Stephen Picken, "TUDelft", and Prof. Stefania Panero, "La Sapienza", for the fruitful discussion on the paper and on the ink preparation respectively. The Shell Sustainable Mobility Project and Alistore European Research Institute have substantially contributed to this work by their financial support.

References

[1] M. Winter, J.O. Besenhard, M.E. Spahr, P. Novák, Adv. Mater. 10 (1998) 725–763.
[2] U. Kasavajjula, C. Wang, A.J. Appleby, J. Power Sources 163 (2007) 1003–1039.
[3] J. Ryu, J. Kim, Y. Sung, S. Oh, Electrochem. Solid State Lett. 7 (2004) A306–A309.
[4] I.-S. Kim, P.N. Kumta, G.E. Blomgren, Electrochem. Solid State Lett. 3 (2000) 493–496.
[5] I.-S. Kim, G.E. Blomgren, P.N. Kumta, J. Power Sources 130 (2004) 275–280.
[6] Z.P. Guo, J.Z. Wang, H.K. Liu, S.X. Dou, J. Power Sources 146 (2005) 448–451.
[7] H. Uono, B.-C. Kim, T. Fuse, M. Ue, J.-I. Yamaki, J. Electrochem. Soc. 153 (2006).
[8] J. Maranchi, A. Hepp, A. Evans, N. Nuhfer, P. Kumta, J. Electrochem. Soc. 153 (2006) A1246–A1253.
[9] M. Holzapfel, H. Buqa, L.J. Hardwick, M. Hahn, A. Würsig, W. Scheifele, P. Novák, R. Kütz, C. Veit, F.-M. Petrat, Electrochim. Acta 52 (2006) 973–978.
[10] M. Holzapfel, H. Buqa, W. Scheifele, P. Novák, F.-M. Petrat, Chem. Commun. (2005) 1566–1568.
[11] H. Li, X. Huang, L. Chen, Z. Wu, Y. Liang, Electrochem. Solid State Lett. 2 (1999) 547–549.
[12] J. Graetz, C. Ahn, R. Yazami, B. Fultz, Electrochem. Solid State Lett. 6 (2003) A194–A197.
[13] M. Uehara, J. Suzuki, K. Tamura, K. Sekine, T. Takamura, J. Power Sources 146 (2005) 441–444.
[14] J. Maranchi, A. Hepp, P. Kumta, Electrochem. Solid State Lett. 6 (2003) A198–A201.
[15] S. Bourderau, T. Brousse, D. Schleich, J. Power Sources 82 (1999) 233–236.
[16] D. Larcher, S. Beattie, M. Morcrette, K. Edström, J.-C. Jumas, J.-M. Tarascon, J. Mater. Chem. 17 (2007) 3759–3772.
[17] J. Yang, B.F. Wang, K. Wang, Y. Liu, J.Y. Xie, Z.S. Wen, Electrochem. Solid-State Lett. 6 (2003) A154–A156.
[18] M. Kaneko, M. Nakayama, M. Wakihara, J. Solid State Electrochem. 11 (2007) 1071–1076.
[19] H. Buqa, M. Holzapfel, F. Krumeich, C. Veit, P. Novák, J. Power Sources 161 (2006) 617–622.
[20] W.-R. Liu, M.-H. Yang, H.-C. Wu, S.M. Chiao, N.-L. Wu, Electrochem. Solid State Lett. 8 (2005).

[21] J. Drofenik, M. Gaberscek, R. Dominko, F.W. Poulsen, M. Mogensen, S. Pejovnik, J. Jamnik, Electrochim. Acta 48 (2003) 883–889.
[22] W. Cannon, S. Danforth, J. Haggerty, R. Marra, J. Am. Ceram. Soc. 65 (1982) 330–335.
[23] W. Cannon, S. Danforth, J. Flint, J. Haggerty, R. Marra, J. Am. Ceram. Soc. 65 (1982) 324–330.
[24] J. Schoonman, E.M. Kelder, J. Power Sources 68 (1997) 65–68.
[25] K. Yamada, N. Sato, T. Fujino, C.G. Lee, I. Uchida, J.R. Selman, J. Solid State Electrochem. 3 (1999) 148–153.
[26] M. Valvo, U. Lafont, D. Munao, E.M. Kelder, J. Power Sources 189 (2009) 297–302.
[27] J. van Erven, D. Munao, Z. Fu, T. Trzeciak, R. Janssen, E. Kelder, J.C.M. Marijnissen, Kona 27 (2009) 157–173.
[28] K. Pal, A.K. Banthia, D.K. Majumdar, Mater. Manuf. Process. 21 (2006) 877–882.
[29] A. Magasinski, P. Dixon, B. Hertzberg, A. Kvit, J. Ayala, G. Yushin, Nat. Mater. (2010).
[30] A. Jaworek, Powder Technol. 176 (2007) 18–35.
[31] M. Obrovac, L. Krause, J. Electrochem. Soc. 154 (2007) A103–A108.
[32] C.-H. Doh, H.-M. Shin, D.-H. Kim, Y.-D. Jeong, S.-I. Moon, B.-S. Jin, H.-S. Kim, K.-W. Kim, D.-H. Oh, A. Veluchamy, J. Alloys Compd. 461 (2008) 321–325.
[33] J. Li, L. Christensen, M.N. Obrovac, K.C. Hewitt, J.R. Dahn, J. Electrochem. Soc. 155 (2008) A234–A238.
[34] J. Li, R.B. Lewis, J.R. Dahn, Electrochem. Solid-State Lett. 10 (2007) A17–A20.
[35] A.G. Zakharov, A.N. Prusov, Fibre Chem. 38 (2006) 325–336.
[36] H. Miyamoto, M. Umemura, T. Aoyagi, C. Yamane, K. Ueda, K. Takahashi, Carbohydr. Res. 344 (2009) 1085–1094.
[37] C. Yamane, M. Mori, M. Saito, K. Okajima, Polym. J. 28 (1996) 1039–1047.
[38] N.S. Hochgatterer, M.R. Schweiger, S. Koller, P.R. Raimann, T. Wöhrle, C. Wurm, M. Winter, Electrochem. Solid-State Lett. 11 (2008) A76–A80.
[39] J.-S. Bridel, T. Azais, M. Morcrette, J.-M. Tarascon, D. Larcher, Chem. Mater. 22 (2010) 1229–1241.
[40] P. Cordier, F. Tournilhac, C. Soulié-Ziakovic, L. Leibler, Nature 451 (2008) 977–980.
[41] M. Gorman, J. Chem. Educ. 34 (1957) 304–306.